Hindawi
Mathematical Problems in Engineering
Volume 2019, Article ID 4843738, 14 pages
https://doi.org/10.1155/2019/4843738

Research Article

The Use of a Pendulum Dynamic Mass Absorber to Protect a Trilithic Symmetric System from the Overturning

Angelo Di Egidio,[1] **Andrea M. de Leo**,[1] **and Alessandro Contento**[2]

[1]*Dipartimento di Ingegneria Civile, Edile-Architettura e Ambientale, University of L'Aquila, Italy*
[2]*Department of Civil and Environmental Engineering, University of Illinois at Urbana-Champaign, USA*

Correspondence should be addressed to Angelo Di Egidio; angelo.diegidio@univaq.it

Received 16 October 2018; Revised 10 December 2018; Accepted 18 December 2018; Published 14 January 2019

Academic Editor: Francesco Aymerich

The trilith consists of two vertical elements (columns) supporting a horizontal element (lintel). The understanding of the dynamic behaviour of triliths is an important step towards their preservation and starts with the knowledge of the dynamics of rigid blocks. A passive method based on a dynamic mass absorber is used to protect a trilith from overturning. The protection system is modelled as a pendulum, hinged on the lintel, with the mass lumped at the end. The equations of rocking motion, uplift and the impact conditions are obtained for the coupled system trilith-mass absorber. An extensive parametric analysis is performed with the aim to compare the behaviour of the system with and without the pendulum, under impulsive one-sine (or one-cosine) base excitations. In order to point out the effectiveness of the protection system, overturning spectra, providing the amplitude of the excitation versus its frequency, are obtained. The pendulum mass absorber results effective in avoiding overturning in specific ranges of the frequency of the excitation. However, outside these ranges the mass absorber never compromises the safety of the trilith.

1. Introduction

The dynamical behaviour of block-like structures has focused the interest of many researchers in the last fifty years. The reason is that several elements such as hospital equipment, storage boxes, and in some cases historical monument and art objects, show a rocking motion typical of block-like structures when subjected to earthquakes. Therefore, the initial studies on this kind of structures used two-dimensional models to analyze the dynamics of symmetric blocks subject to earthquakes excitations [1, 2].

Even though the response of block-like structures to earthquakes remains a central topic [3, 4], other kinds of ground excitation have been considered in subsequent studies. Random and harmonic excitations were discussed in [5–9], respectively. Several papers enriched the original two-dimensional symmetric model of rigid block. Non-symmetric rigid blocks are modelled in [10, 11]. In [12, 13], instead, the possibility for combined slide-rocking motions is contemplated. The transitions among the different phases of motions are analyzed in details in [14–16]. An alternative three-dimensional formulation for the rigid block motion that considers the rocking and the spinning over one vertex of the block-like structure is presented in [17–19].

In the last years, a topic of broad interest is the protection of block-like structures. Several papers investigated different methodologies and devices. The simplest method is the anchorage of the block-like structures, as in [20, 21] where a semi-active control of the rocking motion is also considered. Instead, an active control method is used in [22]. The most investigated protection methodology is the use of base isolation [10, 23]. In the majority of the paper on base isolation, the element is constrained to remain on the base since the sliding is usually prevented. In [24], instead, the block-like element is allowed to slide or rock partially outside the oscillating base. The research presented in [25] investigates the effectiveness of base isolation for block-like elements at different levels of a multi-story frame. Another protection methodology for block-like elements is the use of Tuned Mass Dampers (TMD). The effectiveness of a TMD constituted by a single degree of freedom oscillating mass connected to the block with a linear visco-elastic device is

analyzed in [26–28]. The use of a different kind of TMD is proposed in [29] where the motion is controlled using a sloshing water damper. Some recent studies proved, with both deterministic [30, 31] and probabilistic [32] approaches, the effectiveness of pendulum damping systems to control the rocking motion.

Some papers considered multiple blocks, either stacked or in the configuration of a trilith. A contact model for rigid blocks is proposed in [33]. In [4, 34], the rocking of two stacked rigid block is analyzed considering different possible patterns and deriving the equations of motion for each pattern. The identification of the minimum amplitude that leads to the overturning of multiple block systems is studied in [35, 36]. A few papers are focused on the dynamics of triliths. The main difference among them is in the modeling of the impact between two elements of the trilith and with the ground. The studies presented in [37, 38] make use of specific formulations that are discussed in [33, 39], respectively. In [40], instead, the loss of energy associated with the impact is used to define the initial conditions for the post-impact motion. The angular momentum-impulse theorem applied on one column of the frame before and after the impact is used in [41] to define the maximum coefficient of restitution of the rocking frame. In particular, in the same paper, an equivalent single block model is used to analyze the motion of a multicolumn rocking frame. Using the same model, in [42], it is demonstrated that the stability of the rigid frame increase with the weight of the lintel.

In this paper a passive method of motion control, based on the use of dynamic mass absorber is used to protect from overturning a trilithic structure with equal columns and generic shaped and positioned lintel. The only restriction considered on the geometry of the lintel is that the contact zones with the top of the columns is horizontal. In trilithic structures with equal columns, the columns rotate of the same angle and the lintel undergoes only to translational motion. The adopted protection system is constituted by a mass absorber, modelled as a pendulum hinged on the lintel with the mass lumped at the end. The equations of motion of the trilith coupled with the mass absorber are obtained; the uplift and the impact conditions are derived in a rigorous way, contrarily to what done in [31].

An extensive parametric analysis is performed with the aim to compare the behaviour of the system with and without pendulum, under impulsive external excitations. Specifically, in order to point out the efficiency of the pendulum mass absorber, a one-sine (or one-cosine) base excitations is considered. Overturning spectra, providing the amplitude of the excitation versus its frequency, are obtained for a wide class of triliths characterized by different geometrical properties, with and without pendulum mass absorbers. The results show the effectiveness of this kind of protection in avoiding overturning.

2. Mechanical Model

The mechanical system is constituted by two equal columns and a generic shaped and positioned lintel. The only restriction considered on the geometry of the lintel is that the contact zones with the top of the columns is horizontal. The pendulum mass absorber is hinged to the lintel in a generic point and it has a lumped mass connected at its end point. The columns and the lintel are assumed to be made of the same material and of unitary depth (the dimension orthogonal the plane containing the trilith). The three bodies of the trilith are modelled as rigid blocks. A sufficiently larger friction coefficient is assumed to prevent the slipping between columns and ground and between columns and lintel as in [41]. So, the trilith can undergo only rocking motion. The two equal columns of the trilith rotate of the same angle, and the lintel undergoes only a translation (it does not rotate, see [41]). Figure 1 shows the geometrical parameters characterizing the mechanical system; $\overline{G}_i$, $(i = 1, \ldots, 3)$ are the mass centers of the three rigid blocks constituting the trilith, and $\overline{G}_4$ is the position of the mass of the pendulum. The pendulum is hinged on the lintel at point $\overline{o}$.

Under an impulsive base excitation, the overturning of blocks happens either directly, without any impact between the base and the ground, or after the first impact. The dynamic mass absorber intercepts a fraction of the initial inertial forces acting on the block before the uplift. In this way, the dynamic mass absorber reduces the amplitude of the rocking angle of the block in the first rocking motion cycle. The pendulum device does not work as a tuned mass damper, since it is not tuned to any frequency characterizing the system

2.1. Full Contact Equation of Motion. If the external excitation is not capable of uplifting the columns, the trilith remains at rest. In this case, only the pendulum oscillates. The equation of motion describing the oscillation of the pendulum is the classical one:

$$m_4 g l \sin(\psi) + m_4 l^2 \ddot{\psi} + m_4 \ddot{x}_g l \cos(\psi) = 0 \tag{1}$$

where $\psi = \psi(t)$ is the oscillating angle of the pendulum; m_4 and l are its mass and length; g and $\ddot{x}_g$ (see Figure 2) are the gravity and the external base accelerations, respectively.

2.2. Rocking Equations of Motion. When the external excitation is able to uplift the columns, the rocking motion of the trilithic system starts. Two sets of rocking equations describes the motion around the base corners of the columns. In this Section only the equations describing the rocking around the left corners of the columns are described (Figure 2). Those describing the motion around the right corners of the columns are in Appendix A.

In the following $\mathbf{r}_{G_j}$ $(j = 1, \ldots, 4)$ are the vectors of the centres of mass positions of the four bodies of the system (the columns, the lintel and the mass of the pendulum) with respect to point O, which is the origin of an inertial frame initially coincident with point A (Figure 1). A vector $\mathbf{r}_{PQ}$ describes the position of a generic point P with respect to a generic point Q. The overbar denotes quantities related to the initial position of the trilith, and quantities without overbar refer to generic positions assumed during the rocking motion.

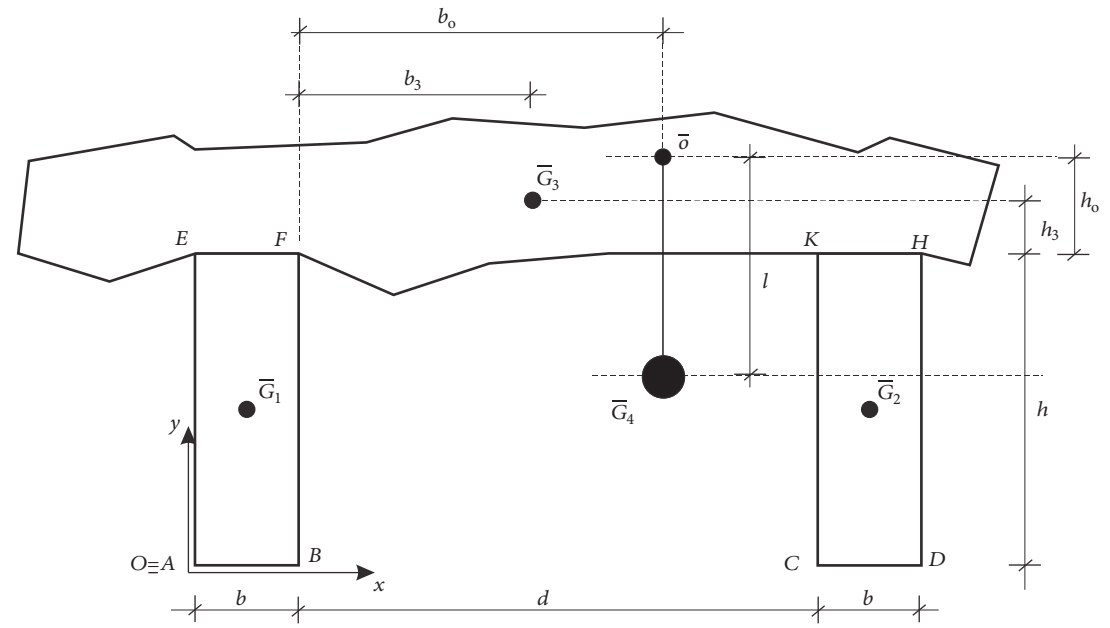

Figure 1: Geometrical characterization of the trilith.

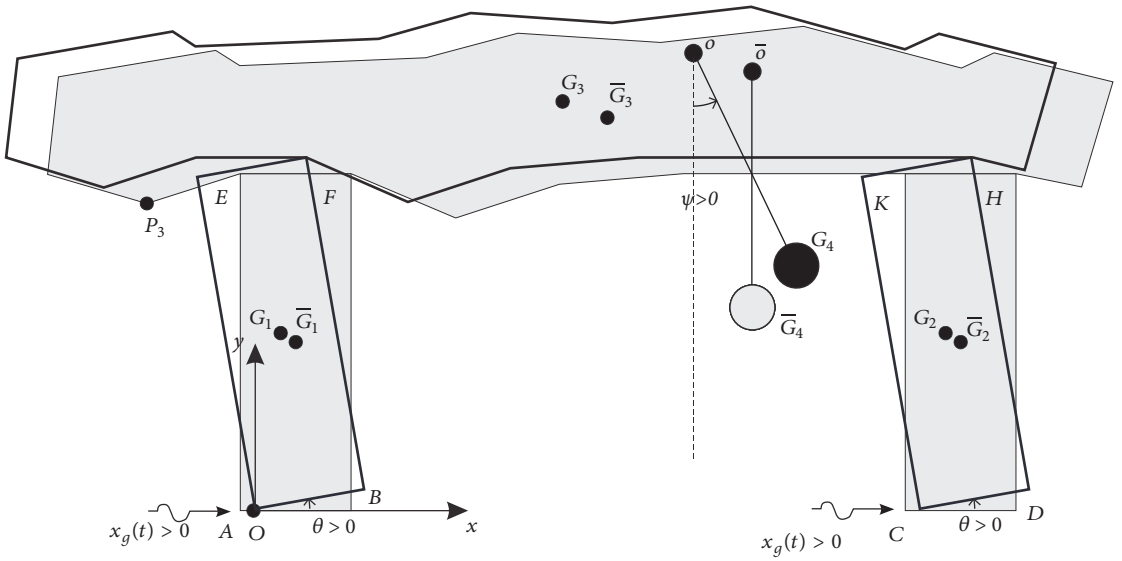

Figure 2: Rocking motion of the trilith around the left base corner.

The positions of the mass centres in the reference configuration read:

$$\begin{aligned}
\overline{\mathbf{r}}_{G_1} &= \overline{\mathbf{r}}_{AG_1} \\
\overline{\mathbf{r}}_{G_2} &= \overline{\mathbf{r}}_{AC} + \overline{\mathbf{r}}_{CG_2} \\
\overline{\mathbf{r}}_{G_3} &= \overline{\mathbf{r}}_{AF} + \overline{\mathbf{r}}_{FG_3} \\
\overline{\mathbf{r}}_{G_4} &= \overline{\mathbf{r}}_{AF} + \overline{\mathbf{r}}_{FO} + \overline{\mathbf{r}}_{OG_4}
\end{aligned} \tag{2}$$

Their actual positions during the motion are:

$$\begin{aligned}
\mathbf{r}_{G_1} &= \mathbf{x}_g + \mathbf{R}_\vartheta \overline{\mathbf{r}}_{AG_1} \\
\mathbf{r}_{G_2} &= \mathbf{x}_g + \overline{\mathbf{r}}_{AC} + \mathbf{R}_\vartheta \overline{\mathbf{r}}_{CG_2} \\
\mathbf{r}_{G_3} &= \mathbf{x}_g + \mathbf{R}_\vartheta \overline{\mathbf{r}}_{AF} + \overline{\mathbf{r}}_{FG_3} \\
\mathbf{r}_{G_4} &= \mathbf{x}_g + \mathbf{R}_\vartheta \overline{\mathbf{r}}_{AF} + \overline{\mathbf{r}}_{FO} + \mathbf{R}_\psi \overline{\mathbf{r}}_{OG_4}
\end{aligned} \tag{3}$$

where $\mathbf{x}_g = \{x_g(t), 0, 0\}^T$ is the base external displacement and $\mathbf{R}_\vartheta$ and $\mathbf{R}_\psi$ are two tensors describing the rigid rotation of the columns $\theta(t)$ and the rotation of the pendulum $\psi(t)$ (see Figure 2), respectively. They read:

$$\mathbf{R}_\vartheta = \begin{pmatrix} \cos(\theta) & -\sin(\theta) & 0 \\ \sin(\theta) & \cos(\theta) & 0 \\ 0 & 0 & 1 \end{pmatrix},$$

$$\mathbf{R}_{\psi} = \begin{pmatrix} \cos(\psi) & -\sin(\psi) & 0 \\ \sin(\psi) & \cos(\psi) & 0 \\ 0 & 0 & 1 \end{pmatrix} \tag{4}$$

Taking into account Eq. (4), with geometric considerations (see Figure 2), the vectors that define the actual positions of the four bodies with respect to the reference inertial frame with origin in O can be explicitly written as:

$$\begin{aligned}
\mathbf{r}_{G_1} &= \left\{ x_g + \frac{1}{2} b\cos(\theta) - \frac{1}{2} h\sin(\theta), \frac{1}{2} b\sin(\theta) \right. \\
&\quad \left. + \frac{1}{2} h\cos(\theta), 0 \right\}^T \\
\mathbf{r}_{G_2} &= \left\{ x_g + b + d + \frac{1}{2} b\cos(\theta) \right. \\
&\quad \left. - \frac{1}{2} h\sin(\theta), \frac{1}{2} b\sin(\theta) + \frac{1}{2} h\cos(\theta), 0 \right\}^T \\
\mathbf{r}_{G_3} &= \left\{ x_g + b_3 + b\cos(\theta) - h\sin(\theta), h_3 + b\sin(\theta) \right. \\
&\quad \left. + h\cos(\theta), 0 \right\}^T \\
\mathbf{r}_{G_4} &= \left\{ x_g + b_o + b\cos(\theta) - h\sin(\theta) + l\sin(\psi), h_o \right. \\
&\quad \left. + b\sin(\theta) + h\cos(\theta) - l\cos(\psi), 0 \right\}^T
\end{aligned} \tag{5}$$

In order to obtain the equations of motion the Lagrangian approach is used. The kinetic energy of the system, during the rocking motion reads:

$$T = \frac{1}{2} \sum_{j=1}^{4} m_i \left(\dot{\mathbf{r}}_{G_j} \cdot \dot{\mathbf{r}}_{G_j} \right) + \frac{1}{2} \sum_{j=1}^{2} J_{G_j} \left(\dot{\boldsymbol{\theta}} \cdot \dot{\boldsymbol{\theta}} \right) \tag{6}$$

where $m_j\,(j = 1, \ldots, 4)$ are the masses of the four bodies; $J_{G_j}\,(j = 1, 2)$ are the polar inertia of the two columns with respect to their centres of mass; $\dot{\mathbf{r}}_{G_j}$ are obtained by time-deriving Eq. (5); $\dot{\boldsymbol{\theta}}$ is the time-derivation of the axial rotation vector $\boldsymbol{\theta} = \{0, 0, \theta(t)\}^T$. It is worth observing that no rotational inertia of the lumped mass of the pendulum is considered. Moreover, the rotational inertia of the lintel is not taken into account, since the lintel undergoes only translational motion when the trilith has equal columns.

The potential energy of the system during the rocking motion is defined as:

$$V = -\sum_{j=1}^{4} m_j \left(\mathbf{r}_{G_j} - \tilde{\mathbf{r}}_{G_j} \right) \cdot \mathbf{g} \tag{7}$$

where $\tilde{\mathbf{r}}_{G_j}$, $(j = 1, \ldots, 4)$ are the positions of the four bodies which correspond to the minimum potential energy (being constants, they disappear in the process of time derivation needed for the writing of the equations of motion); $\mathbf{g} = \{0, -g, 0\}^T$ is the gravity acceleration vector.

By defining the Lagrangian of the system $L = T - V$, the equations of rocking motion are obtained as:

$$\begin{aligned}
& g\left(m_1 + m_3 + m_4\right)\left(b\cos(\theta) + h\sin(\theta)\right) \\
& \quad + l m_4 \dot{\psi}^2 \left(b\cos(\theta - \psi) + h\sin(\theta - \psi)\right) \\
& \quad - \left(m_1 + m_3 + m_4\right) \ddot{x}_g \left(h\cos(\theta) + b\sin(\theta)\right) \\
& \quad + \frac{1}{2} \ddot{\theta} \left(\left(b^2 + h^2\right)\left(m_1 + 2\left(m_3 + m_4\right)\right) + 4 J_G \right) \\
& \quad - l m_4 \ddot{\psi} \left(b\sin(\theta - \psi) + h\cos(\theta - \psi)\right) = 0 \\
& - l m_4 \ddot{\theta} \left(b\sin(\theta - \psi) + h\cos(\theta - \psi)\right) \\
& \quad + l m_4 \dot{\theta}^2 \left(-b\cos(\theta - \psi) + h\sin(\theta - \psi)\right) \\
& \quad + l m_4 \left(g\sin(\psi) + l\ddot{\psi} + \cos(\psi)\ddot{x}_g\right) = 0
\end{aligned} \tag{8}$$

where $m_2 = m_1$ is assumed. The equations of motion for the rocking around the right base corners are obtained similarly (Appendix A).

3. Uplift Condition

The minimum value of the external excitation a_{up} which induce the uplift of the trilith, around the left corner of the columns can be found assuming $\theta = \dot{\theta} = \ddot{\theta} = 0$ in Eq. (8). As:

$$a_{up} = \frac{2\gamma l \dot{\psi}^2 \left(\lambda\sin(\psi) - \cos(\psi)\right) - g\left(\gamma\lambda\sin(2\psi) + \gamma\cos(2\psi) + \gamma + 2\mu + 2\right)}{-\lambda\left(\gamma + 2\mu + 2\right) + \gamma\lambda\cos(2\psi) - \gamma\sin(2\psi)} \tag{9}$$

where:

$$\begin{aligned}
m_3 &= \mu m_1, \\
m_4 &= \gamma m_1 \\
\lambda &= \frac{h}{b}
\end{aligned} \tag{10}$$

When $\gamma = 0$ (i.e. in the case without the pendulum), Eq. (9) reduces to:

$$a_{up} = \frac{g}{\lambda} \tag{11}$$

Eqation (11) shows that in the case without the pendulum, the uplift acceleration does not depend on the mass of the linthel, but only on the slendereness λ of the columns, as

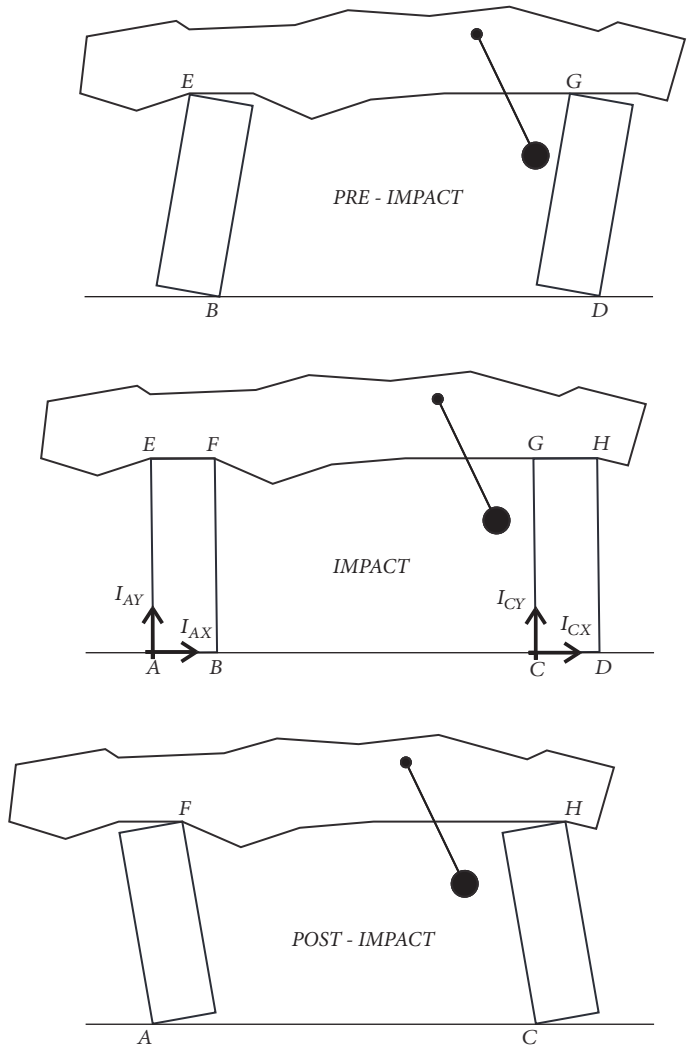

Figure 3: Impulses in an impact that occurs when the trilith rocks around the right base corners and successively re-uplifts around the left base corners.

already found in [41]. The uplift condition referring to the right corners of the columns can be obtained in a similar way.

4. Impact Conditions

When the angle $\theta(t)$ vanishes, an impact takes place. To correctly describe the dynamics of the system, its post-impact state has to be solved. Let's assume that the pre-impact angular velocity of the trilith is counterclockwise and the impact occurs at points A, C, F, H (see Figure 3, where only the base impulses are drawn). The unkowns of the problem are six, namely the four impulse at the impact points and the post impact angular velocities of the trilith and of the pendulum. Below the superscript (+) will denote always post-impact quantities, whereas the superscript (-) will denote pre-impact quantities.

In general, the impulse at point j I_j is defined as:

$$I_j = \lim_{\Delta t_i \longrightarrow 0} \int_{\Delta t_i} F_j \, dt \tag{12}$$

where F_j is the impact force and Δt_i is the duration of the impact. All non-impulsive forces (e.g., inertia forces and self-weights) are considered negligible compared with the impact forces. Proceeding as in [43], the six equations describing the impact problem are:

(1) Linear momentum along x-axis for the whole system

$$\begin{aligned} I_{AX} + I_{CX} = &- \left[h \left(m_1 + m_3 + m_4 \right) \left(\dot{\theta}^- - \dot{\theta}^+ \right) \right. \\ &\left. + m_4 l \cos\left(\psi \right) \left(\dot{\psi}^+ - \dot{\psi}^- \right) \right] \end{aligned} \tag{13}$$

(2) Linear momentum along y-axis for the whole system

$$\begin{aligned} I_{AY} + I_{CY} = &- \left[b \left(m_1 + m_3 + m_4 \right) \left(\dot{\theta}^- + \dot{\theta}^+ \right) \right. \\ &\left. + m_4 l \sin\left(\psi \right) \left(\dot{\psi}^+ - \dot{\psi}^- \right) \right] \end{aligned} \tag{14}$$

(3) Moment of momentum about point F for the left column

$$-I_{AY}b + I_{AX}h = \left(m_1\frac{h^2}{4} - J_G\right)\left(\dot{\theta}^+ - \dot{\theta}^-\right) + \frac{b^2}{4}m_1\left(\dot{\theta}^- + \dot{\theta}^+\right) \tag{15}$$

(4) Moment of momentum about point H for the right column

$$-I_{CY}b + I_{CX}h = \left(m_1\frac{h^2}{4} - J_G\right)\left(\dot{\theta}^+ - \dot{\theta}^-\right) + \frac{b^2}{4}m_1\left(\dot{\theta}^- + \dot{\theta}^+\right) \tag{16}$$

(5) Moment of momentum about point A for the whole system

$$I_{CY}(b+d) = -b\left(\dot{\theta}^- + \dot{\theta}^+\right)\left[m_4\left(b + b_0 + l\sin(\psi)\right) + m_1\left(b + \frac{d}{2}\right) + m_3\left(b + b_3\right)\right] + \left(\dot{\theta}^- - \dot{\theta}^+\right)\left[2J_G + \frac{h^2}{2}m_1 + hm_4\left(h + h_0 - l\cos(\psi)\right) + h\left(h + h_3\right)m_3\right] + -lm_4\left(\dot{\psi}^+ - \dot{\psi}^-\right) \cdot \left[(b + b_0)\sin(\psi) - (h + h_0)\cos(\psi) + 1\right] \tag{17}$$

(6) Moment of momentum about o (the pivot point) for the pendulum

$$0 = m_4\left(l^2\left(\dot{\psi}^+ - \dot{\psi}^-\right) + bl\sin(\psi)\left(\dot{\theta}^+ + \dot{\theta}^-\right) + hl\cos(\psi)\left(\dot{\theta}^- - \dot{\theta}^+\right)\right) \tag{18}$$

The solution of these equations gives the four impulse at the impact points (whose expressions are not reported) and the post impact angular velocities $\dot{\theta}^+$ and $\dot{\psi}^+$. Specifically, the post-impact angular velocity of the columns reads:

$$\dot{\theta}^+ = -\frac{-4J_G + m_4\left(b^2 + h^2\right)\cos(2\psi) + \left(b^2 - h^2\right)\left(m_1 + 2m_3 + m_4\right)}{4J_G + m_4\left(b\cos(\psi) + h\sin(\psi)\right)^2 + \left(b^2 + h^2\right)\left(m_1 + 2m_3\right)}\dot{\theta}^- \tag{19}$$

When $m_4 = 0$ (i.e. in the case without the pendulum), Eq.(19) reduces to:

$$\dot{\theta}^+ = -\frac{-4J_G + \left(b^2 - h^2\right)\left(m_p + 2m_t\right)}{4J_G + \left(b^2 + h^2\right)\left(m_p + 2m_t\right)}\dot{\theta}^- \tag{20}$$

Equation (20) provides the same result found in [41]. The post impact angular velocity of the pendulum reads:

$$\dot{\psi}^+ = \dot{\psi}^- - \frac{2b\left(h\left(m_1 + 2\left(m_3 + m_4\right)\right)\left(\mathrm{b}\cos(\psi) + h\sin(\psi)\right) + 4J_G\sin(\psi)\right)}{l\left(\left(b^2 + h^2\right)\left(m_1 + 2m_3\right) + 2m_4\left(\mathrm{b}\cos(\psi) + h\sin(\psi)\right)^2 + 4J_G\right)}\dot{\theta}^- \tag{21}$$

As it is possible to observe, the equations of motion in Eq. (8), the expression of the uplift acceleration in Eq. (9) and the impact conditions reported in Eqs. (19)–(21) do not depend neither on the position of the pivot point o of the pendulum, nor on the position of the center of mass of the lintel G_3. Hence, the pendulum mass damper can be freely positioned without compromising its effectiveness in the protection of the trilith from the overturning.

The impact conditions referring to an impact that occurs at points B, D, E, K (see Figure 2), can be obtaine in a similar way.

5. Parametric Analyses

An extensive parametric analysis is performed to point out the efficiency of the pendulum mass absorber under external excitation. The system is excited by an impulsive one-sine (or one-cosine) base excitation. Overturning spectra, providing the amplitude of the excitation versus its frequency, are obtained for a broad class of triliths characterised by different geometrical properties. The overturning spectra are built evaluating the overturning amplitude of the one-sine (or one-cosine) excitation which corresponds to the first overturning occurrence. Several regions where the block could regain stability could exist over this amplitude, but they are not analyzed in this paper. An original code has been implemented for the numerical integrations of the equations of motion needed to construct the spectra. Particular care has been devoted to the detection of impacts and to the choice of the integration time step. The length of the pendulum is taken $l = (2/3)h$ (Figure 1), since some preliminary analyses showed that the behaviour of the trilith with the pendulum

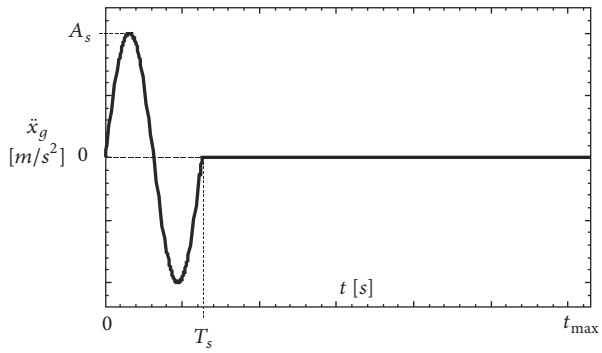

Figure 4: Characteristics of the one sine-pulse excitation.

only marginally depends on the length of the mass absorber, provided its length is $l \geq 1/3h$.

5.1. Base Excitations. Mainly a one-sine impulsive excitation is the base excitation considered in the analyses. The same kind of excitation is commonly used in the study of the dynamics of bi-dimensional rigid blocks ([5, 19, 21]). Specifically, the pulse-type one-sine excitation used in the analyses reads:

$$\ddot{x}_g(t) = \begin{cases} A_s \sin(\Omega t) & 0 \leq t \leq T_s \\ 0 & 0 \leq t \leq T_s \end{cases} \tag{22}$$

where $\Omega = 2\pi/T_s$ is the circular frequency of the impulsive excitation, T_s is the period of the one-cycle impulse, and A_s is its amplitude (see Figure 4). Here, t_{max} is the maximum time used in the numerical integrations, and it is taken at least ten times the period T_s of the one-cycle pulse. However, some results are obtained by considering a one-cosine excitation. The similarities among results obtained by the two type of excitations, has suggested to use mainly one of them. Specifically, the pulse-type one-cosine excitation used in the analyses reads:

$$\ddot{x}_g(t) = \begin{cases} A_s \cos(\Omega t) & 0 \leq t \leq T_s \\ 0 & 0 \leq t \leq T_s \end{cases} \tag{23}$$

The use of the one-sine base excitation is often used to describe near fault seismic excitations.

It is worth observing that the paper is a first attempt to investigate the effectiveness of a dynamic mass absorber in protecting a trilithic structure from overturning. Therefore, the paper does not approach the study of the seismic response of the coupled system, but investigates the sensitivity of the coupled system to several parameters.

5.2. Overturning Spectrum. The first analysis refers to a trilith with fixed geometrical characteristics $\lambda = 5$, and the mass ratios considered are $\gamma = 0.3$ and $\mu = 1.0$ (see Eq. (10)). For the given mass ratios, the pendulum has a mass that is smaller or equal to the 10% of the total mass ot the trilith (the 10% of the total mass is obtained when the lintel and colums have

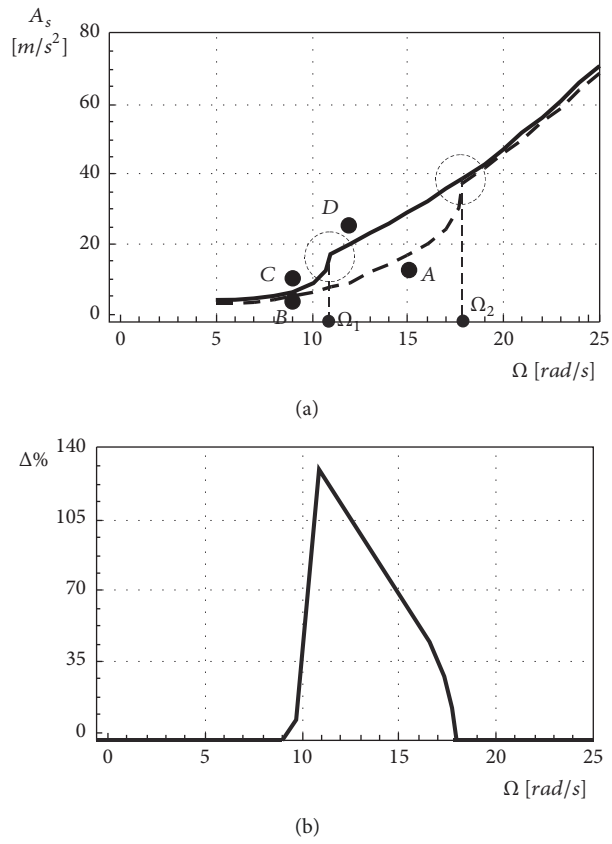

Figure 5: Overturning spectrum: (a) overturning spectrum for one-sine excitation (solid line: trilith with pendulum; dashed line: trilith without pendulum); (b) percentage gain Δ; ($\lambda = 5, B = 0.6cm, \gamma = 0.3, \mu = 1$).

the same mass). Figure 5(a) shows two overturning spectra, one referring to the case with the mass absorber (solid line), and the other to the case without mass absorber (dashed line). The two spectra are almost coincident, except that in a specific range of the circular frequencies of the one-sine pulse excitation. Specifically, between the circular frequencies Ω_1 and Ω_2 the pendulum has positive effects on the overturning of the block. In fact, in this range, the presence of the mass absorber increases the amplitude of the excitation required to overturn the block. Outside this range, the presence of the pendulum has not sensible effects. In correspondence of the angular discontinuities of the overturning spectra, inside the dashed circles, a substantial change of the overturning phenomenon of the block occurs. More in detail, before and after the discontinuity, the block overturns with two different modes, coherently with the findings of [19], as discussed in the next paraghraphs. The region between the spectra of the triliths with and without pendulum mass absorber is called gain range (or advantage range) in the following and the corresponding area between the two spectra is named gain or safe region. Figure 5 clearly shows the efficiency of the dynamic mass absorber through the graph of the percentage gain provided by the pendulum. Calling A_{yp} and A_{np} the overturning amplitudes of the block with and without the

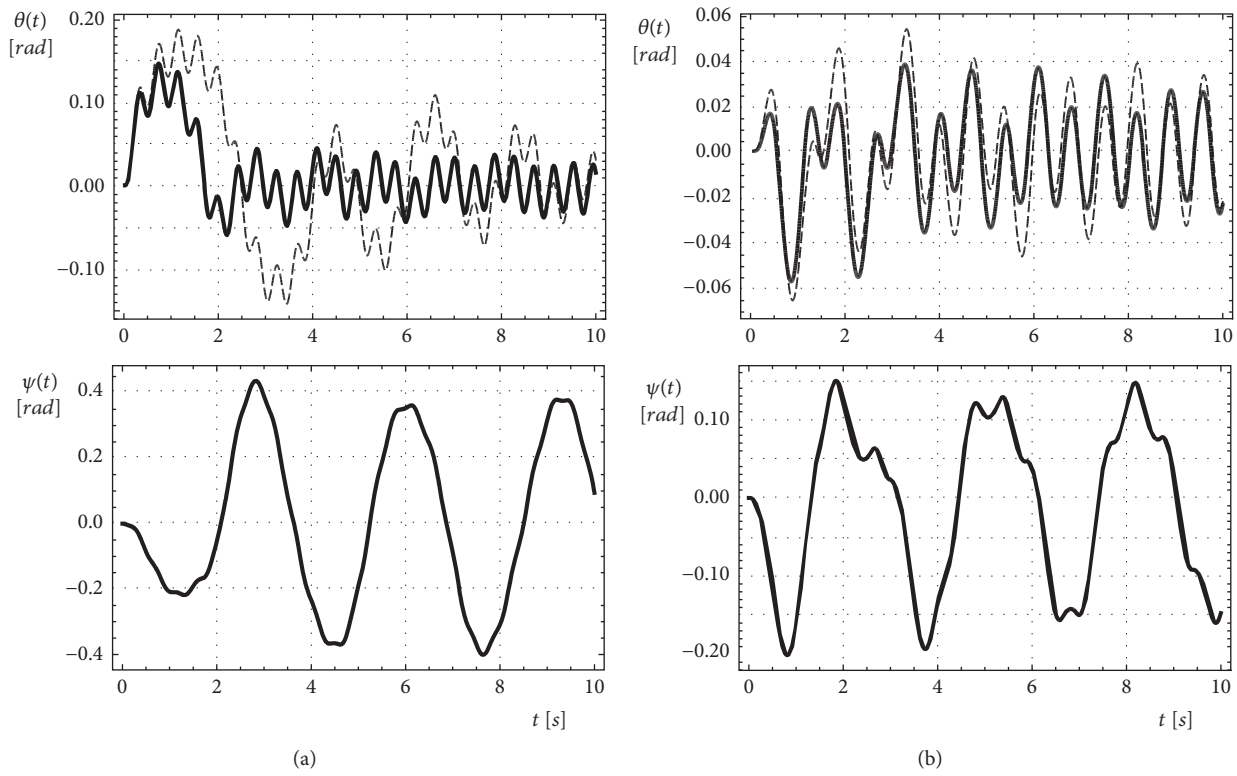

FIGURE 6: Time-histories of the angles $\theta(t)$ and $\psi(t)$: (a) Case labelled with A in Figure 5 ($A_s = 19m/s^2, \Omega = 15rad/s$); (b) Case labelled with B in Figure 5 ($A_s = 4m/s^2, \Omega = 9rad/s$); ($\lambda = 5, B = 0.6cm, \gamma = 0.3, \mu = 1$); solid line: trilith with pendulum; dashed line: trilith without pendulum.

pendulum, respectively, the gain provided by the dynamic mass absorber is evaluated as $\Delta = 100 \times (A_{yp} - A_{np})/A_{np}$. Specifically, in Figure 5(b) the percentage gain obtained for the overturning spectrum of Figure 5(a) is shown. Although the increase in the excitation amplitude able to overturn the block in presence of the dynamic mass absorber is almost constant (i.e. the distance between the spectra is almost constant), the percentage gain changes considerably, almost reaching 140% for $\Omega = 11rad/s$.

Figure 6 shows the time-histories of the angles $\theta(t)$, describing the rocking motion of the trilith, and of the angle $\psi(t)$, accounting for the oscillation of the pendulum. The two couples of graphs refer to the cases labelled with A and B in Figure 5. In particular, point A is inside the range where the presence of the pendulum increases the safety of the trilith. Figure 6(a) shows the $\theta(t)$ and $\psi(t)$ time histories of systems with (solid line) and without (dashed line) pendulum mass absorber for case A. The time-history of $\theta(t)$ for the case without pendulum (dashed line) displays two fundamental frequencies. In this case, the mass absorber reduces the rocking oscillations since the pendulum oscillates in counter-phase with respect to the component of the rocking motion that has the lowest frequency (greater period). On the contrary, the case labeled as B does not present any apparent advantage since it is located outside the advantage range (Figure 5). The time history in Figure 6(b) shows that, for this latter case, the rocking angle is only marginally affected by the presence of the mass absorber.

In Figure 7 the time-histories of the angle $\theta(t)$, describing the rocking motion of the trilith equipped with the mass absorber, are shown. The two graphs refer to the cases labelled with C and D in Figure 5. In particular, point C is located before the discontinuity point, above the spectrum of the system with the mass absorber (*i.e.* before the frequency Ω_1), whereas point D is located after the discontinuity point, above the same spectrum (*i.e.* after the frequency Ω_1). As expected the time-histories manifest two different ways of overturning of the trilith. More in detail, in Figure 7(a) (point C) the overturning of the trilith happens impacting the ground, whereas in Figure 7(b) (point D) the overturning occurs without impacting the ground, thus confirming the findings pesented in [19] also for trilithic systems coupled with pendulum mass absorbers.

5.3. The Role of the Mass of the Pendulum. In this section the dependence of the motion on the mass ratio of the pendulum, γ (Eq. (10)), is investigated, for the case of one-sine excitation. The results are shown as overturning spectra organized in matrix form in Figure 8. The rows refer to different values of the slenderness λ (Eq. (10)), and the columns refer to different mass ratios γ of the pendulum.

The comparison of the spectra obtained for systems with the same slenderness shows that an increase in the mass ratio γ always results in an improvement in the behaviour of the trilith. For any slenderness, the safe regions enlarge when the pendulum is added to the system. By observing

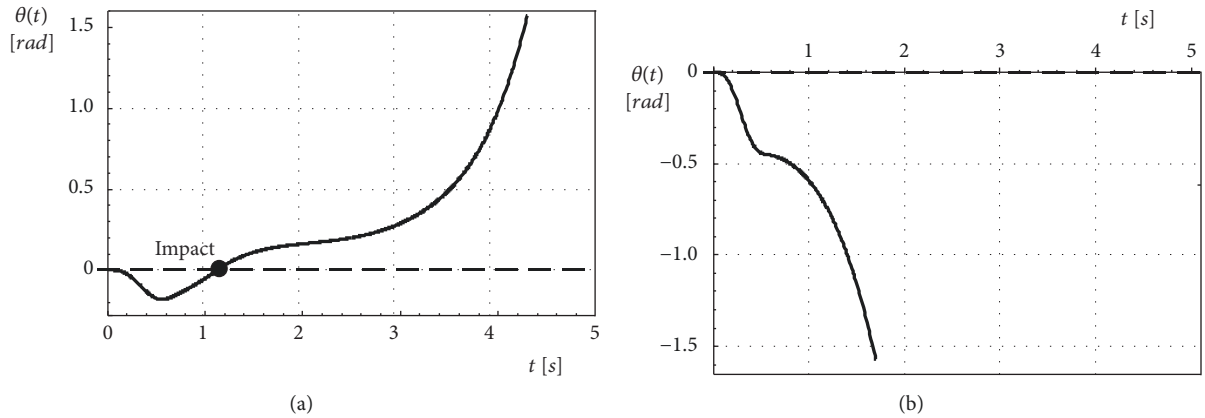

FIGURE 7: Time-histories of the angles $\theta(t)$: (a) Case labelled with C in Figure 5 ($A_s = 10m/s^2, \Omega = 9rad/s$); (b) Case labelled with D in Figure 5 ($A_s = 25m/s^2, \Omega = 11rad/s$); ($\lambda = 5, B = 0.6cm, \gamma = 0.3, \mu = 1$).

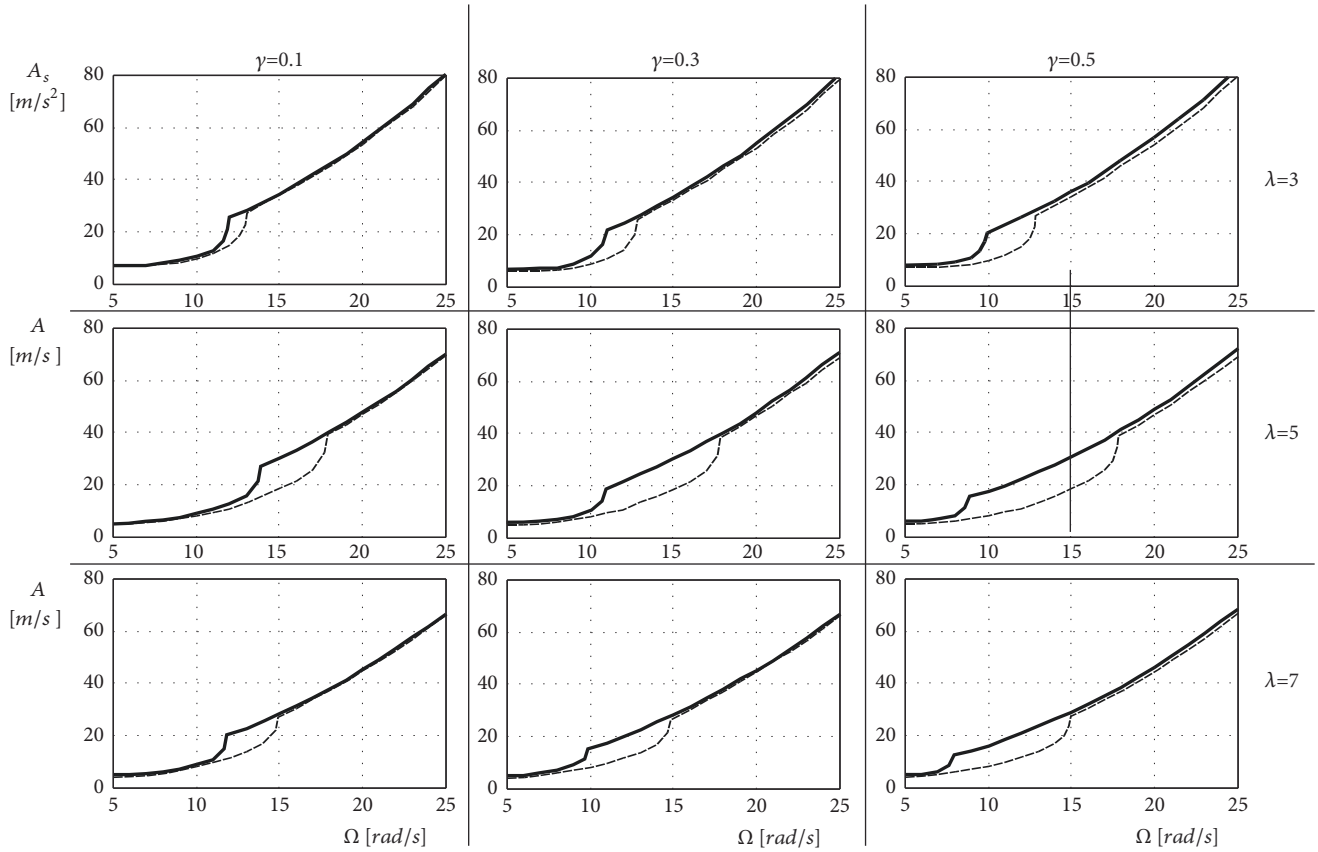

FIGURE 8: Overturning spectra for one-sine excitation ($B = 0.6cm, \mu = 1$); solid line: trilith with pendulum; dashed line: trilith without pendulum.

the overturning spectra along the columns of Figure 8, it is evident that the pendulum effect on the behaviour of the trilith is not directly proportional to the slenderness. The area of the gain regions does not grow up monotonically as the slenderness λ increases. The safety of the system improves as it increase λ from $\lambda = 3$ to $\lambda = 5$ but it reduces with a further increase of slenderness, $\lambda = 7$.

5.4. The Role of the Base of the Columns. The role of the base b of the columns of the trilith in the behaviour of the system also investigated. Figure 9 shows the overturning spectra organized in matrix form, similarly to Figure 8. The rows refer to different slenderness λ of the trilith, whereas the columns refer to different base $b$of the columns. Below a pendulum with $\gamma = 0.3$ is always considered. Results indicate

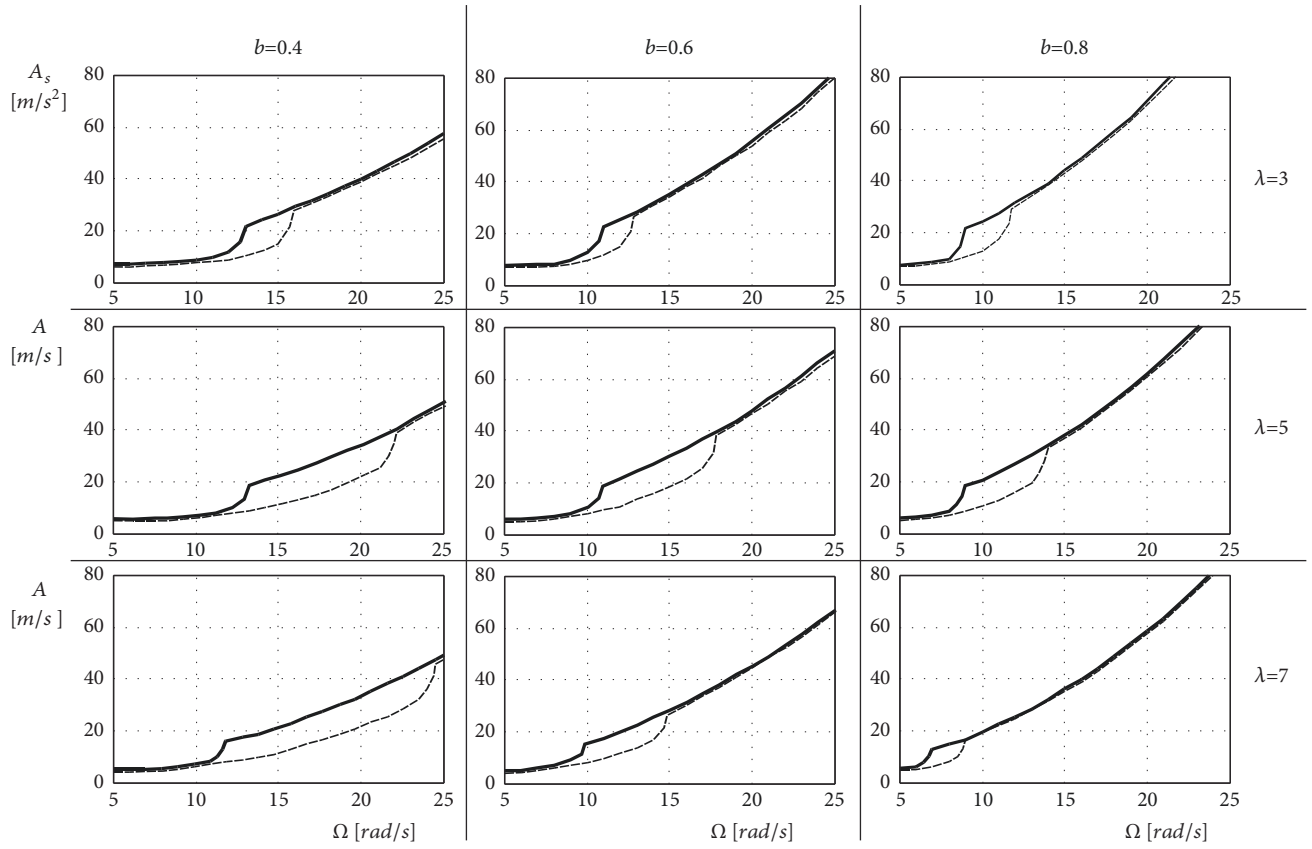

FIGURE 9: Overturning spectra for one-sine excitation ($\gamma = 0.3$, $\mu = 1$); solid line: trilith with pendulum; dashed line: trilith without pendulum.

that an increase of the columns base b corresponds to an overall reduction in the gain range extension of the (one-sine) excitation frequency. On the contrary, to an increase of the slenderness λ does not correspond a monotonic enlargment of the gain regions. This fact mainly occurs for column base $b > 0.4m$.

In Figure 10 the overturning spectra obtained by exciting the trilith with a one-cosine excitation are shown. The results refer to $b = 0.4m$ and therefore, they can be compared directly with the result of the first left column of Figure 9. As it is possible to observe, the amplitude of the one-cosine excitation is in general higher than that of the one-sine excitation. Also the jumps that overturning curves undergo when a change of the overturning mode manifests itself (see Section 5.2), are greater than the ones observed in case of one-sine excitation. However, the same evolution for an increasing slenderness of the columns of the trilith is observed. Specifically, to an increase of λ an increase of the gain region occurs, as happens for one-sine excitation (see the first left column of Figure 9). Since the effects on the overturning curves of the one-cosine excitation are very similar to those observed for the one-sine one, we omit to report further results on the one-cosine pulse.

5.5. The Role of the Mass of the Lintel. The last analysis is aimed to understand the effects of the mass ratio μ of the lintel on the rocking motion. Figure 11 shows results of motion simulations of triliths with fixed slenderness, base and mass ratio of the pendulum ($\lambda = 5$, $b = 0.6m$, $\gamma = 0.3$), under a one-sine excitation. As it can be observed, as the mass of the lintel increases the gain frequency range shrinks. This finding is in accordance with the results shown in Section 5.3, where the larger is the mass ratio of the pendulum, the better is the performance of the system. Even if a fixed mass ratio $\gamma = 0.3$ is considered, the ratio of the mass of the pendulum on the total mass of the trilith decreases when the mass of the lintel increases.

It can be observed that the advantage regions where the passive control is effective are mostly located between $\Omega = 10$ and $\Omega = 15$ *rad/s* (0.6-0.4 *s* in terms of periods), for the one-sine excitation. In such a range of frequencies, most of the earthquakes have consistent spectral power content. Moreover, the use of the pendulum mass absorber never worsen the dynamics of the system (i.e., it never leads to an overturn for an amplitude of the excitation lower than the one that overturns the trilith without pendulum). Additionally, the effectiveness of the pendulum does not depend on its position, and marginally depends on its length (provided that the length is $l \geq 1/3h$). Consequently there is a wide range of possibilities to choose the position and the length of the pendulum in such a way that minimize the interference of the pendulum with the structure and its aesthetic.

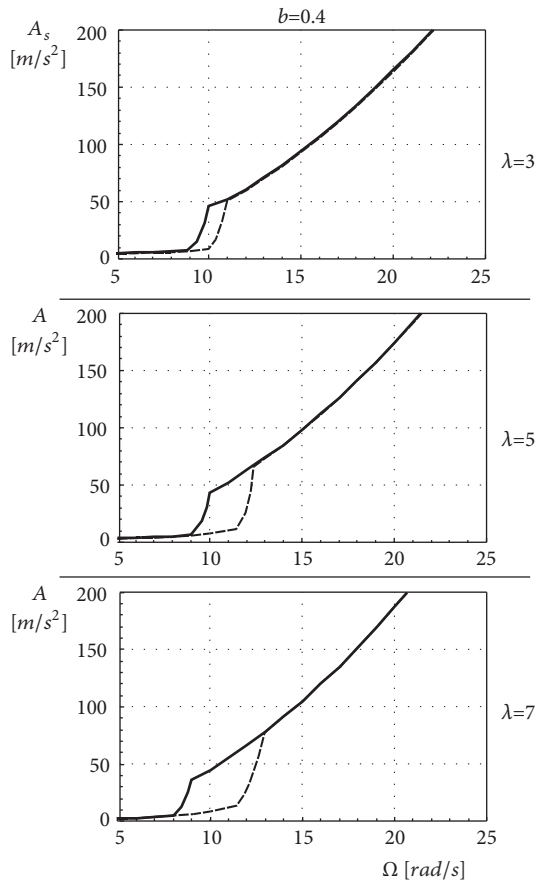

Figure 10: Overturning spectra for one-cosine excitation ($\gamma = 0.3, \mu = 1$); solid line: trilith with pendulum; dashed line: trilith without pendulum.

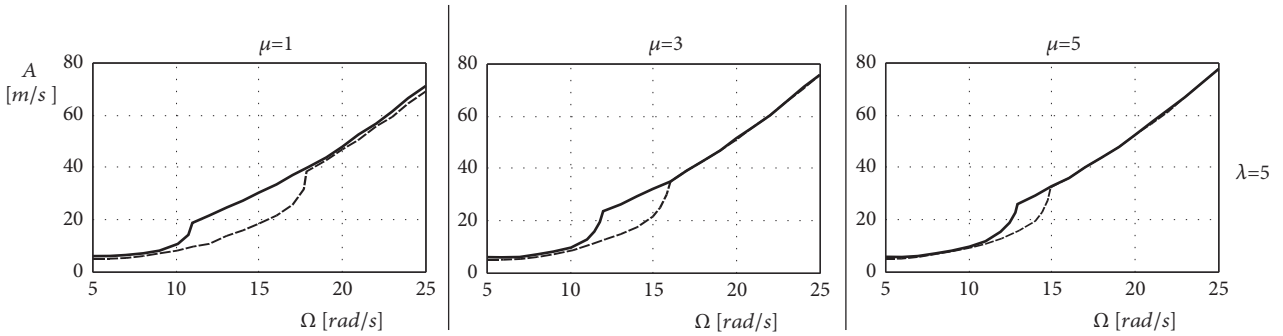

Figure 11: Overturning spectra for one-sine excitation ($\lambda = 5, B = 0.6cm, \gamma = 0.3$); solid line: trilith with pendulum; dashed line: trilith without pendulum.

6. Conclusions

The study presented the evaluation of the effectiveness of a passive control method based on the use of a dynamic mass absorber to avoid the overturning of a thrilith with equal columns and generic shaped and positioned lintel. The protection system has been modelled as a pendulum hinged on the lintel with its mass lumped at the end. The equations of rocking motion of the trilith coupled with the pendulum mass absorber, the exact uplift conditions, and impact conditions have been obtained.

An extensive parametric analysis has been performed to compare the behaviour of the system with and without pendulum under impulsive one-sine (or one-cosine) base excitations. The comparison is made using overturning spectra that provide the amplitude of the excitation able to overturn the trilith versus the frequency of the excitation. These spectra, obtained for a wide class of triliths characterized by different geometrical and mechanical properties, prove the effectiveness of the mass absorber to avoid overturning. Specifically, there is a range of the frequencies of the pulse-type excitation where the presence of the pendulum improves

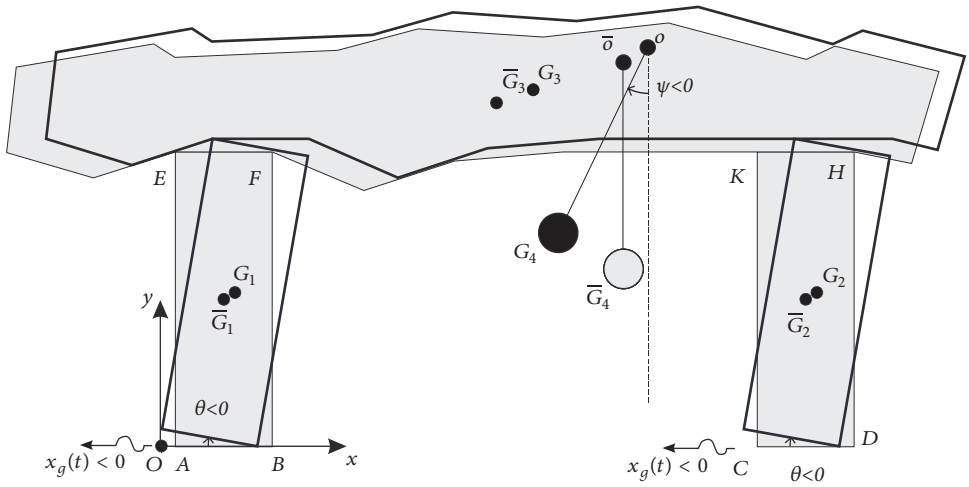

Figure 12: Rocking motion of the trilith around the right base corner.

the behaviour of the system. Inside this regions, a larger amplitude of the excitation is required to overturn the trilith. The width of these gain ranges sensibly depends on the geometrical characteristics of the trilith and on the ratio between the mass of the pendulum and the total mass of the system. In particular, the width of the gain ranges/regions can be enlarged by increasing the mass of the pendulum.

It is important to remark that the addition of the pendulum mass absorber never has a negative effect on the system. In fact, outside the advantage regions, the overturning spectra of the system with and without the dynamic mass absorber are almost coincident.

Appendix

A. Rocking Motion around the Right Base Corner

In this section the equations of motion for a trilith rocking around the right base corners (see Figure 12) of the columns are reported.

A.1. Rocking Equations of Motion. The equations of rocking motion around the right base corners of the columns read:

$$
\begin{aligned}
&- g\left(m_1 + m_3 + m_4\right)\left(b\cos\left(\theta\right) + h\sin\left(\theta\right)\right)\\
&- lm_4\dot{\psi}^2\left(b\cos\left(\theta-\psi\right) + h\sin\left(\theta-\psi\right)\right)\\
&- \left(m_1 + m_3 + m_4\right)\ddot{x}_g\left(h\cos\left(\theta\right) - b\sin\left(\theta\right)\right)\\
&+ \frac{1}{2}\ddot{\theta}\left(\left(b^2 + h^2\right)\left(m_1 + 2\left(m_3 + m_4\right)\right) + 4J_G\right)\\
&+ lm_4\ddot{\psi}\left(b\sin\left(\theta-\psi\right) - h\cos\left(\theta-\psi\right)\right) = 0\\
lm_4&\ddot{\theta}\left(b\sin\left(\theta-\psi\right) - h\cos\left(\theta-\psi\right)\right)\\
&+ lm_4\dot{\theta}^2\left(b\cos\left(\theta-\psi\right) + h\sin\left(\theta-\psi\right)\right)\\
&+ lm_4\left(g\sin\left(\psi\right) + l\ddot{\psi} + \cos\left(\psi\right)\ddot{x}_g\right) = 0
\end{aligned}
\tag{A.1}
$$

Data Availability

No data were used to support this study.

Conflicts of Interest

The authors declare that they have no conflicts of interest.

References

[1] M. Aslam, D. T. Scalise, and W. G. Godden, "Earthquake rocking response of rigid blocks," *Journal of the Structural Engineering Division (ASCE)*, vol. 106, no. 2, pp. 377–392, 1980.

[2] G. W. Housner, "The behavior of inverted pendulum structures during earthquakes," *Bulletin of the Seismological Society of America*, vol. 53, no. 2, pp. 403–417, 1963.

[3] A. Pompei, A. Scalia, and M. A. Sumbatyan, "Dynamics of rigid block due to horizontal ground motion," *Journal of Engineering Mechanics*, vol. 124, no. 7, pp. 713–717, 1998.

[4] P. D. Spanos, P. C. Roussis, and N. P. A. Politis, "Dynamic analysis of stacked rigid blocks," *Soil Dynamics and Earthquake Engineering*, vol. 21, no. 7, pp. 559–578, 2001.

[5] A. N. Kounadis, "Parametric study in rocking instability of a rigid block under harmonic ground pulse: A unified approach," *Soil Dynamics and Earthquake Engineering*, vol. 45, pp. 125–143, 2013.

[6] P. D. Spanos, A. Di Matteo, A. Pirrotta, and M. Di Paola, "Rocking of rigid block on nonlinear flexible foundation," *International Journal of Non-Linear Mechanics*, vol. 94, pp. 362–374, 2017.

[7] P. D. Spanos and A.-S. Koh, "Rocking of rigid blocks due to harmonic shaking," *Journal of Engineering Mechanics*, vol. 110, no. 11, pp. 1627–1642, 1984.

[8] P. D. Spanos and A.-S. Koh, "Analysis of block random rocking," *Soil Dynamics and Earthquake Engineering*, vol. 5, no. 3, pp. 178–183, 1986.

[9] C.-S. Yim, A. K. Chopra, and J. Penzien, "Rocking response of rigid blocks to earthquakes," *Earthquake Engineering & Structural Dynamics*, vol. 8, no. 6, pp. 565–587, 1980.

[10] I. Caliò and M. Marletta, "Passive control of the seismic rocking response of art objects," *Engineering Structures*, vol. 25, no. 8, pp. 1009–1018, 2003.

[11] A. Contento and A. Di Egidio, "Investigations into the benefits of base isolation for non-symmetric rigid blocks," *Earthquake Engineering & Structural Dynamics*, vol. 38, no. 7, pp. 849–866, 2009.

[12] U. Andreaus, "Sliding-uplifting response of rigid blocks to base excitation," *Earthquake Engineering & Structural Dynamics*, vol. 19, no. 8, pp. 1181–1196, 1990.

[13] H. W. Shenton and N. P. Jones, "Base excitation of rigid bodies. I: formulation," *Journal of Engineering Mechanics*, vol. 117, no. 10, pp. 2286–2306, 1991.

[14] H. W. Shenton III, "Criteria for initiation of slide, rock, and slide-rock rigid-body modes," *Journal of Engineering Mechanics*, vol. 122, no. 7, pp. 690–693, 1996.

[15] T. Taniguchi, "Non-linear response analyses of rectangular rigid bodies subjected to horizontal and vertical ground motion," *Earthquake Engineering & Structural Dynamics*, vol. 31, no. 8, pp. 1481–1500, 2002.

[16] C. C. Tung, "Initiation of motion of a free-standing body to base excitation," *Earthquake Engineering & Structural Dynamics*, vol. 36, no. 10, pp. 1431–1439, 2007.

[17] A. Di Egidio, R. Alaggio, A. Contento, M. Tursini, and E. Della Loggia, "Experimental characterization of the overturning of three-dimensional square based rigid block," *International Journal of Non-Linear Mechanics*, vol. 69, pp. 137–145, 2015.

[18] A. Di Egidio, D. Zulli, and A. Contento, "Comparison between the seismic response of 2D and 3D models of rigid blocks," *Earthquake Engineering and Engineering Vibration*, vol. 13, no. 1, pp. 151–162, 2014.

[19] J. Zhang and N. Makris, "Rocking response of free-standing blocks under cycloidal pulses," *Journal of Engineering Mechanics*, vol. 127, no. 5, pp. 473–483, 2001.

[20] R. Ceravolo, M. L. Pecorelli, and L. Zanotti Fragonara, "Semi-active control of the rocking motion of monolithic art objects," *Journal of Sound and Vibration*, vol. 374, pp. 1–16, 2016.

[21] N. Makris and J. Zhang, "Rocking response of anchored blocks under pulse-type motions," *Journal of Engineering Mechanics*, vol. 127, no. 5, pp. 484–493, 2001.

[22] G. Simoneschi, C. Olivieri, A. M. de Leo, and A. Di Egidio, "Pole placement method to control the rocking motion of rigid blocks," *Engineering Structures*, vol. 167, pp. 39–47, 2018.

[23] A. Di Egidio and A. Contento, "Base isolation of slide-rocking non-symmetric rigid blocks under impulsive and seismic excitations," *Engineering Structures*, vol. 31, no. 11, pp. 2723–2734, 2009.

[24] A. Di Egidio and A. Contento, "Seismic response of a non-symmetric rigid block on a constrained oscillating base," *Engineering Structures*, vol. 32, no. 10, pp. 3028–3039, 2010.

[25] A. Contento and A. Di Egidio, "On the use of base isolation for the protection of rigid bodies placed on a multi-storey frame under seismic excitation," *Engineering Structures*, vol. 62-63, pp. 1–10, 2014.

[26] G. Simoneschi, A. M. de Leo, and A. Di Egidio, "Effectiveness of oscillating mass damper system in the protection of rigid blocks under impulsive excitation," *Engineering Structures*, vol. 137, pp. 285–295, 2017.

[27] A. Di Egidio, A. M. de Leo, and G. Simoneschi, "Effectiveness of mass–damper dynamic absorber on rocking block under one-sine pulse ground motion," *International Journal of Non-Linear Mechanics*, vol. 98, pp. 154–162, 2018.

[28] G. Simoneschi, A. Geniola, A. M. de Leo, and A. Di Egidio, "On the seismic performances of rigid block-like structures coupled with an oscillating mass working as a TMD," *Earthquake Engineering & Structural Dynamics*, vol. 46, no. 9, pp. 1453–1469, 2017.

[29] O. Corbi, "Laboratory investigation on sloshing water dampers coupled to rigid blocks with unilateral constraints," *International Journal of Mechanics and Solids*, vol. 1, no. 1, pp. 29–40, 2006.

[30] L. Collini, R. Garziera, K. Riabova, M. Munitsyna, and A. Tasora, "Oscillations Control of Rocking-Block-Type Buildings by the Addition of a Tuned Pendulum," *Shock and Vibration*, vol. 2016, 2016.

[31] A. M. de Leo, G. Simoneschi, C. Fabrizio, and A. Di Egidio, "On the use of a pendulum as mass damper to control the rocking motion of a rigid block with fixed characteristics," *Meccanica*, vol. 51, no. 11, pp. 2727–2740, 2016.

[32] P. Brzeski, T. Kapitaniak, and P. Perlikowski, "The use of tuned mass absorber to prevent overturning of the rigid block during earthquake," *International Journal of Structural Stability and Dynamics*, vol. 16, no. 10, 1550075, 21 pages, 2016.

[33] U. Andreaus and P. Casini, "Dynamics of three-block assemblies with unilateral deformable contacts. Part 1: Contact modelling," *Earthquake Engineering & Structural Dynamics*, vol. 28, no. 12, pp. 1621–1636, 1999.

[34] I. N. Psycharis, "Dynamic behaviour of rocking two-block assemblies," *Earthquake Engineering & Structural Dynamics*, vol. 19, no. 4, pp. 555–575, 1990.

[35] A. N. Kounadis and G. J. Papadopoulos, "On the rocking instability of a three-rigid block system under ground excitation," *Archive of Applied Mechanics*, vol. 86, no. 5, pp. 957–977, 2016.

[36] A. N. Kounadis, "On the rocking complex response of ancient multispondyle columns: a genious and challenging structural system requiring reliable solution," *Meccanica*, vol. 50, no. 2, pp. 261–292, 2015.

[37] U. Andreaus and P. Casini, "Dynamics of three-block assemblies with unilateral deformable contacts. Part 2: Actual application," *Earthquake Engineering & Structural Dynamics*, vol. 28, no. 12, pp. 1637–1649, 1999.

[38] A. Sinopoli and V. Sepe, "Coupled motion in the dynamic analysis of a three block structure," *Applied Mechanics Reviews*, vol. 46, no. 11, pp. S185–S197, 1993.

[39] A. Sinopoli, "Kinematic approach in the impact problem of rigid bodies," *Applied Mechanics Reviews*, vol. 42, no. 11, pp. 233–244, 1989.

[40] R. H. Allen, I. J. Oppenheim, A. R. Parker, and J. Bielak, "On the dynamic response of rigid body assemblies," *Earthquake Engineering & Structural Dynamics*, vol. 14, no. 6, pp. 861–876, 1986.

[41] N. Makris and M. F. Vassiliou, "Planar rocking response and stability analysis of an array of free-standing columns capped with a freely supported rigid beam," *Earthquake Engineering & Structural Dynamics*, vol. 42, no. 3, pp. 431–449, 2013.

[42] N. Makris and M. F. Vassiliou, "Are some top-heavy structures more stable?" *Journal of Structural Engineering (United States)*, vol. 140, no. 5, 2014.

[43] E. G. Dimitrakopoulos and A. I. Giouvanidis, "Seismic response analysis of the planar rocking frame," *Journal of Engineering Mechanics*, vol. 141, no. 7, p. 04015003, 2015.